

The nonlinear motion of cells subject to external forces

Aondoyima Ioratum-Uba, Aurore Loisy, Silke Henkes, and Tanniemola B. Liverpool
School of Mathematics, University of Bristol - Bristol BS8 1UG, UK

(Dated: August 2, 2021)

To develop a minimal model for a cell moving in a crowded environment such as in tissue, we investigate the response of a liquid drop of active matter moving on a flat rigid substrate to forces applied at its boundaries. Our model incorporates active stresses due to a prescribed orientation profile of the cytoskeleton, coupling with the substrate, surface tension and imposed boundary forces. We find a highly non-linear response to forces that we characterise using the drop velocity, its shape, and the traction between the drop and the substrate. There are two main modes of motion: a long and thin drop with zero traction in the bulk, mostly occurring under strong stretching forces, and a parabolic drop with finite traction in the bulk, mostly occurring under strong squeezing forces. There is a sharp transition between these two modes as a function of the applied forces and indications of drop break-up where large forces stretch the drop in opposite directions.

Cells are highly adaptable and move themselves around in a variety of different conditions and environments [1–3]. This is essential for biological functions such as wound repair [4], organ development [5], and in pathological processes such as cancer metastasis [6]. Understanding individual cell motility and how it affects collective cell migration is key to understanding these processes. Cell motility is powered by the cytoskeleton, a dynamic network of interlinking protein filaments inside the cell [7–9]. These filaments can collectively form anisotropic liquid crystalline (LC) phases [10].

There are a number of mechanisms by which cell motility occurs. The most studied is cell crawling, which combines the treadmilling (polymerisation/depolymerisation) of cytoskeletal actin filaments, with strong adhesion to the substrate, which has been analysed extensively both experimentally [11–15] and theoretically using hydrodynamic mechanical models [16–18], reaction-diffusion chemical models [19, 20], and in confinement [21, 22]. Even in the absence of actin treadmilling, spontaneous motion is still possible in LC active matter systems [23–27]. In cells the likely source of this type of motion is acto-myosin contractility, where myosin II molecular motors cause actin filaments to slide relative to each other [28, 29] and generate an *active stress* that can be contractile, i.e. positive (or extensile, i.e. negative). Contractility also plays a role in the crawling of cells [30].

A minimal description of cell motility is thus provided by the motion of a drop of anisotropic active LC matter. The possible modes of a such a drop freely moving on a flat rigid substrate have recently been classified by some of us in [31]. We identified three modes: motion due to self-advection of active units along their direction of orientation, motion due to active stresses, and motion due to contact angle mismatch. We also showed that a drop moving purely due to active stresses can do so without exerting traction on the substrate [32]. This type of motion is relevant to fast migration in crowded environments [2, 33], where cellular adhesions are unstable at high strain rates [34]. Crowded environments also lead to significant forces on cells. However, many of the

effects of external forces on cell-motility and migration remain a mystery. These forces, either coming from cell-cell tugging or from outside the cell, are important for the functionality of cells and tissues. Experiments show that external forces can alter cell stiffness, induce migration, alter cell shape, induce remodelling, and alter cell phenotype [35–37]. Hence a better handle on them promises to have a significant impact on our understanding of multicellular systems.

In this letter, therefore, we study the dynamics of an active LC drop on a flat surface under external forces applied at its two ends. We model the anisotropy of the cytoskeleton through an imposed LC director field, and the active stress that this generates. The behaviour is controlled by the ratio \mathcal{A} of the active stress to the winding number of the LC director, as measured from the surface to the top of the drop. We classify the motion of the drop according to (1) the difference between the forces on each end, i.e. whether it is being squeezed or stretched and (2) the sum of the forces applied to its two ends, i.e. if it is being pushed to the right (R) or to the left (L). For a passive drop with zero active stress, $\mathcal{A} = 0$, we find parabolic shapes with simple symmetric behaviour: it moves to the right (or left) if it is pushed in the right (or left) direction unless it is stretched above a critical stretching force where it tends to break up into smaller droplets. For an active drop, $\mathcal{A} > 0$ we find a much richer response to external forces. First, it moves to the R almost all the time except when the sum of forces is large in the L direction and it is being squeezed. We also find a wide variety of shapes. Parabolic shapes are observed only when the the drop is being squeezed. When the drop is being stretched, we find (i) a double humped shape when the sum of forces is strongly to the R, (ii) a flat pancake shape which exerts almost no traction on the surface when the sum of forces is small and (iii) droplet break up when the sum of forces is strongly in the L direction. Changing the sign of \mathcal{A} , equivalent to either flipping the winding number or moving from contractile to extensile stresses, flips the directions $L \leftrightarrow R$.

We model a single cell as a two dimensional incompressible active nematic drop moving on a flat rigid sub-

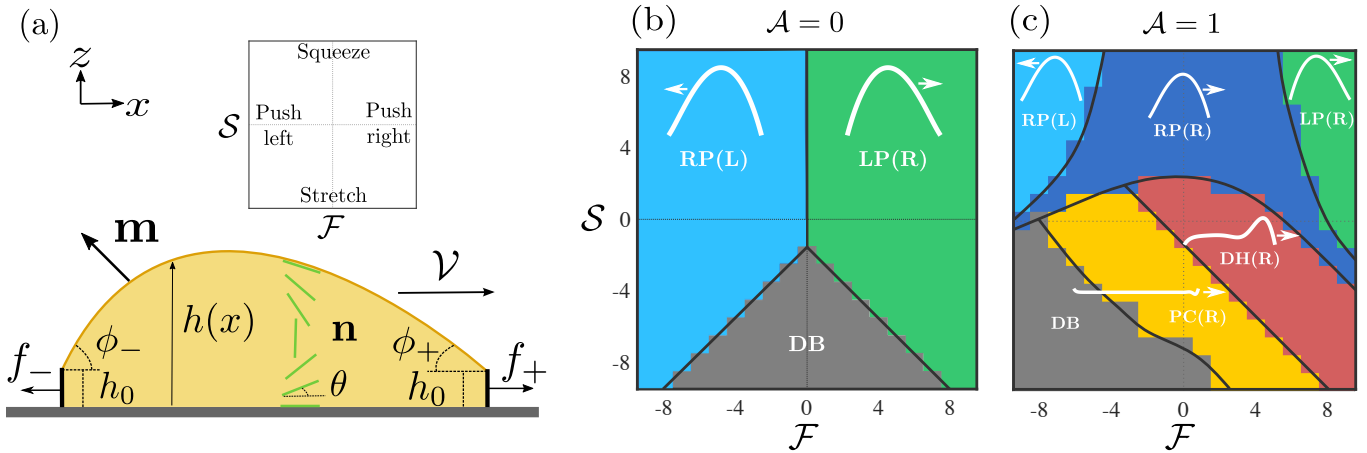


FIG. 1. (a) Schematic showing a drop on a flat surface being pushed/pulled at its boundaries by external forces f_{\pm} (which can also stretch or squeeze the drop), positive f_{+} or f_{-} means that the force is directed to the right. The boundaries are set to be at a height h_0 above the solid substrate ($z = 0$) with corresponding contact angles ϕ_{\pm} . The nematic director is denoted \mathbf{n} . Inset we indicate regions of the phase plane that correspond to stretching, squeezing, or pushing in different directions, where we define push: $\mathcal{F} = f_{+} + f_{-}$ and squeeze: $\mathcal{S} = -(f_{+} - f_{-})$. (b) Schematic phase diagram for a passive drop. The light blue region corresponds to RP(L) right-parabola left-moving drops, green corresponds to LP(R) left-parabola right-moving drops, while droplet breakup DB is grey. (c) Schematic phase diagram for an active drop. New phases include the RP(R) right-parabola right-moving state (dark blue), the DH(R) double-hump right-moving (coral) and the PC(R) pancake right-moving (yellow) states. Characteristic drop shapes are superimposed in white.

strate subject to external forces at its boundaries (Fig. 1 (a)). We work in the (\tilde{x}, \tilde{z}) plane, where the drop is characterised by the height $\tilde{h}(\tilde{x}, \tilde{t})$ of its free surface above the substrate, and moves with velocity \tilde{V} . We use the well established equations of active liquid crystal hydrodynamics [38, 39] where the motion of the coarse grained orientation of elongated units $\mathbf{n} = (\cos \theta, \sin \theta)$, known as the director, is coupled to the fluid velocity $\tilde{\mathbf{u}}$ inside the drop. The velocity satisfies force balance equations at vanishing Reynolds number:

$$\partial_j \tilde{\sigma}_{ij} + \tilde{f}_i = 0, \quad (1a)$$

$$\tilde{\sigma}_{ij} = -\tilde{p}\delta_{ij} + \eta(\partial_i \tilde{u}_j + \partial_j \tilde{u}_i) - \tilde{\alpha} n_i n_j, \quad (1b)$$

where $\tilde{\mathbf{f}} = \tilde{\mathbf{f}}(\tilde{x})$ is the external force per unit height, \tilde{p} is the pressure, $\tilde{\mathbf{u}}$ is the fluid velocity inside the drop, and $\tilde{\alpha}$ is the active stress which represents the coarse-grained stresses generated when cytoskeletal actin filaments slide relative to each other [40, 41]. Following [31, 32], we keep the lowest order gradients in the stress tensor and we work in the strong elastic limit, where dynamic equation for the director reduces to $\nabla^2 \theta$. We anchor the director parallel to the substrate, i.e. $\theta(\tilde{z} = 0) = 0$, and parallel to the free surface with an imposed winding, i.e. $\theta(\tilde{z} = \tilde{h}) = \omega\pi + \arctan(h')$. The winding number $\omega \in \mathbb{Z}^+$ counts the number of half turns of the director across the drop height (Fig. 1). At fixed activity, the winding of the director, through its chirality, breaks the left-right symmetry and sets the preferred direction of motion. With no external forces, at positive activity (extensile drop), the drop moves right for positive winding and left for

negative winding. There is no active contribution to the drop velocity when $\omega = 0$.

The external forces $\tilde{f}_{\tilde{x}} = \tilde{f}_{+}\delta(\tilde{x} - \frac{\tilde{L}}{2}) + \tilde{f}_{-}\delta(\tilde{x} + \frac{\tilde{L}}{2})$, $\tilde{f}_{\tilde{z}} = 0$ are localised at the left and right drop borders, which leads to boundary conditions on the pressure $\tilde{p}(\pm\tilde{L}/2) = \tilde{\pi}_0 \mp \tilde{f}_{\pm}$, where $\tilde{\pi}_0 = 2\gamma\tilde{\phi}/\tilde{L}_0$ is the Laplace pressure generated by the surface tension γ of a symmetric passive drop of length \tilde{L}_0 and contact angle $\tilde{\phi}$. For an active drop with no external forces, π_0 is a constant shift in the pressure. These boundary conditions can be derived by integrating the \tilde{x} component of (1a) with respect to \tilde{x} from $\tilde{L}/2 - \Delta$ to $\tilde{L}/2 + \Delta$ and from $-\tilde{L}/2 - \Delta$ to $-\tilde{L}/2 + \Delta$, with $\Delta > 0$, and taking the limit $\Delta \rightarrow 0^+$. In addition to these boundary conditions, we use a free surface boundary condition for the stress at the free surface: $\tilde{\sigma} \cdot \mathbf{m} = \gamma\kappa\mathbf{m}$, where γ is the surface tension, \mathbf{m} is the unit normal vector (see Fig 1(a)), and $\kappa = \nabla \cdot \mathbf{m}$ is the curvature of the free surface. The interaction of the drop with the rigid substrate is modelled by a partial slip boundary condition: $\tilde{u}_{\tilde{x}} = \tilde{l}_u \tilde{\sigma}_{\tilde{x}\tilde{z}}/\eta$, where \tilde{l}_u is a slip length. We perform calculations in the lubrication approximation [42] for which changes in the height are much smaller than the width.

We derive an integro-differential equation for the steady state drop height \tilde{h} by seeking travelling wave solutions $\tilde{h}(\tilde{x} - \tilde{V}t)$ which must satisfy, from mass conservation, $\int_0^{\tilde{h}} \tilde{u}_{\tilde{x}} d\tilde{z} = \tilde{V}\tilde{h}$, and then using the relation $\tilde{p} = -\gamma\tilde{h}''$, which can be derived by taking the leading order terms of the normal component of the stress boundary condition at the drop free surface. We then convert the resulting integro-differential equation into a

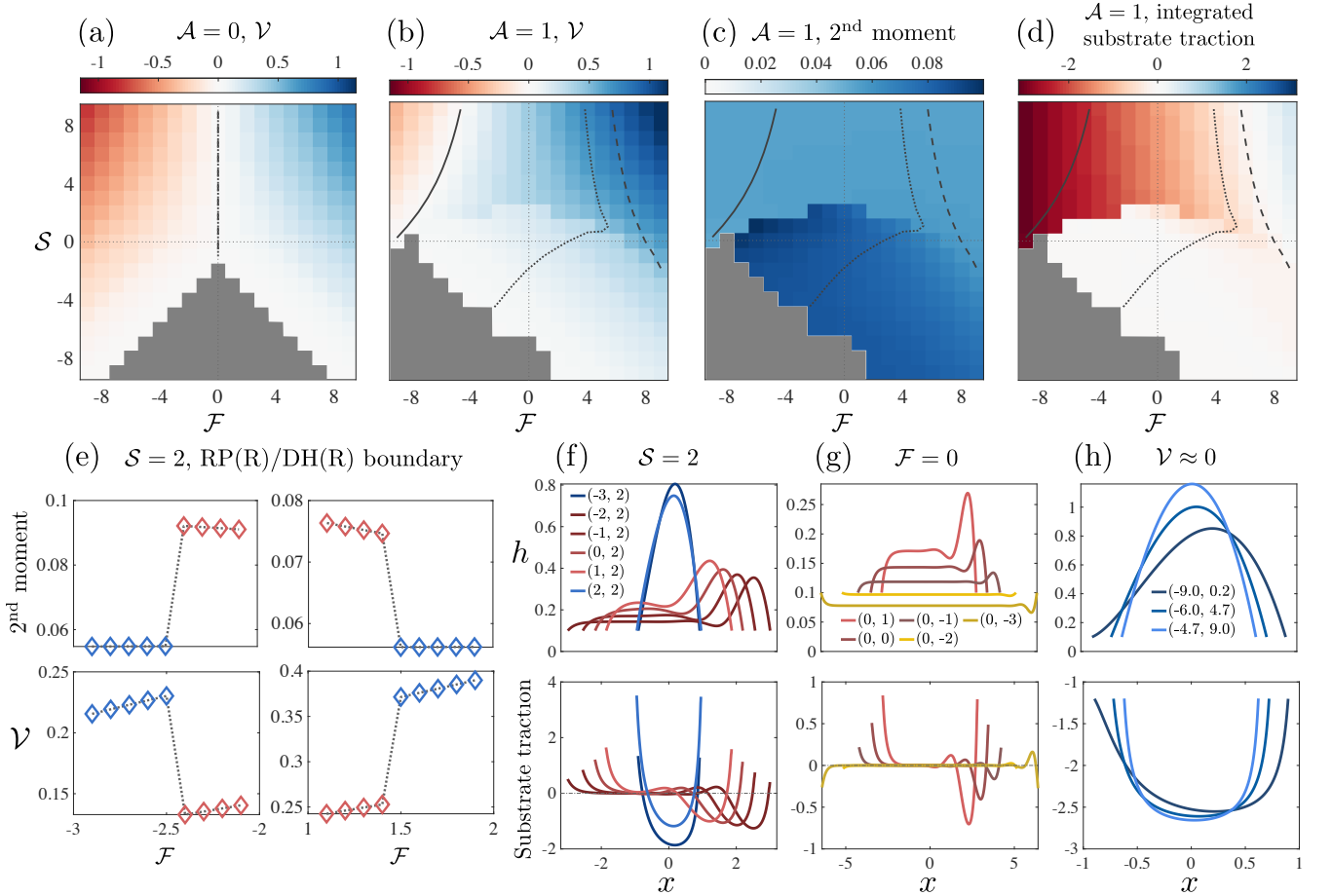


FIG. 2. (a) Velocity of a passive drop. (b) Velocity of an active drop. (c) 2nd moment $\int_{-L/2}^{L/2} (x - \mu_1)^2 h(x) dx$ of an active drop, where $\mu_1 = \int_{-L/2}^{L/2} x h(x) dx$. (d) Traction between the drop and the substrate integrated over 70% of the drop length. Each square represents a single simulation and its colour corresponds to the legend. The solid line in each plot is an isoline corresponding to zero velocity, the dashed line is an isoline corresponding to the 1st moment $\mu_1 = 0$, and the dotted line is an isoline corresponding to the drop having equal contact angles. (e) 2nd moment and velocity \mathcal{V} across the RP(R)/RH(R) boundary, indicating a first order transition. (f) Stable numerical solutions for h (top) and the corresponding traction $\sigma_{xz}|_{z=0}$ (bottom) for $\mathcal{A} = 1$, $\mathcal{S} = 2$, (g) $\mathcal{A} = 1$, $\mathcal{F} = 0$, (h) $\mathcal{V} < 2 \times 10^{-4}$. The colour of each curve matches the colour of its phase in Fig. 1 (c). The legend labels are coordinates in the $(\mathcal{F}, \mathcal{S})$ phase plane.

non-linear ODE. After non-dimensionalisation, we retain the salient parameters activity \mathcal{A} and drop velocity \mathcal{V} ,

$$\mathcal{A} = \frac{\tilde{\alpha} \tilde{L}_x}{4\pi\omega\gamma\epsilon^2}, \quad \mathcal{V} = \frac{\eta \tilde{V}}{\gamma\epsilon^3}, \quad (2)$$

and also height $h = \tilde{h}/\epsilon\tilde{L}_x$, coordinates $x = \tilde{x}/\tilde{L}_x$, $z = \tilde{z}/\epsilon L_x$, slip length $l_u = \tilde{l}_u/\epsilon L_x$, pressure $\pi_0 = \tilde{\pi}_0 \tilde{L}_x/\gamma\epsilon$, and forces $f_{\pm} = \tilde{f}_{\pm} \tilde{L}_x/\gamma\epsilon$, where \tilde{L}_x is a characteristic length scale in the x direction. Then the drop shape satisfies

$$-h'' = C + \frac{1}{2} \left(\int_{-L/2}^x \frac{\mathcal{A}h + \mathcal{V}}{\frac{h^2}{3} + l_u h} d\xi - \int_x^{L/2} \frac{\mathcal{A}h + \mathcal{V}}{\frac{h^2}{3} + l_u h} d\xi \right), \quad (3)$$

where C and the drop velocity \mathcal{V} are integration constants determined by the boundary conditions on pressure to be

$C = \pi_0 + \mathcal{S}/2$, and

$$\mathcal{V} = \left[\int_{-L/2}^{L/2} \frac{\mathcal{A} dx}{\frac{h}{3} + l_u} + \mathcal{F} \right] / \left[\int_{-L/2}^{L/2} \frac{dx}{\frac{h^2}{3} + l_u h} \right], \quad (4)$$

where we have introduced squeeze $\mathcal{S} = -(f_+ - f_-)$ and push $\mathcal{F} = f_+ + f_-$ (pull corresponds to negative push, stretch to negative squeeze). Because equation (3) is a second order equation, we must impose two boundary conditions. Here, we choose to set the height of the drop at its boundary to a finite $h_0 = h(\pm L/2)$, which represents a finite contact area with neighbouring cells or with obstacles. Then equation (3) can be differentiated with respect to x to obtain

$$h''' \left(\frac{1}{3} h^3 + l_u h^2 \right) + \mathcal{A} h^2 = \mathcal{V} h. \quad (5)$$

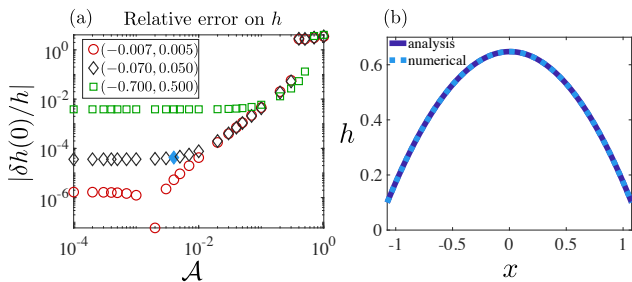


FIG. 3. (a) Relative error between numerical solution and analytic solution at $x = 0$ as a function of \mathcal{A} for $(\mathcal{F}, \mathcal{S}) = (-0.007, 0.005)$ (circles), $(-0.070, 0.050)$ (diamonds), and $(-0.700, 0.500)$ (squares). The diamond coloured in blue at $\mathcal{A} = 0.004$ corresponds to the profile plotted in (b).

The drop length L is determined as part of the solution by requiring that the drop have constant volume Ω : $\int_{-L/2}^{L/2} h dx = \Omega$. The tangential traction exerted by the drop on the substrate is $\sigma_{xz}|_{z=0} = hh'''$. In terms of h alone, using (5), the traction can be written $\sigma_{xz}|_{z=0} = (\mathcal{V} - \mathcal{A}h)/(\frac{1}{3}h + l_u)$.

We obtain solutions to (5) by numerically solving the time dependent version of the force balance equation, $\partial_t h + \partial_x I = 0$, where $I = h'''(\frac{1}{3}h^3 + l_u h^2) + \mathcal{A}h^2 - \mathcal{V}h$, which represents overdamped dynamics of the height evolution. Solving the time dependent problem (starting from a known initial condition) allows us to iteratively evaluate the integrals in equation (4) and gives us the potential to investigate the temporal dynamics of the drop. The steady state of the time evolution, $\partial_t h = 0$, is equivalent to equation (5). We simulate the dynamics until steady state using a Crank-Nicholson algorithm with adaptive time stepping, where the time step is increased as steady state approaches [31]. In the numerics, we apply both height and pressure boundary conditions (converted to boundary conditions on h'') because the time evolution is a fourth order PDE:

$$h(\pm L/2) = h_0, \quad h''(\pm L/2) = \pm f_{\pm} - \pi_0. \quad (6)$$

The boundary conditions on h'' are required for consistency with force balance, however we are in principle free to change the boundary conditions on h . The third derivative term is discretised implicitly, while the other terms are explicitly discretised using finite difference coefficients (see SI at [43] for further details). In all simulations $l_u = 0.05$, $h_0 = 0.1$, $\Omega = 1$, $\pi_0 = 0.9226$, $\omega = 1$, and the spatial step size is 0.002.

The phase diagrams in Fig. 1b-c schematically show the regimes of drop shapes and motility that we find for the passive $\mathcal{A} = 0$ and the active $\mathcal{A} = 1$ case. Figure 2 provides full results for drop velocity, drop shapes and substrate traction.

We first study a passive drop $\mathcal{A} = 0$ (Fig. 1 (b)) and observe two phases of motion, both with finite traction in the bulk: a left-moving right-parabola RP(L) for $\mathcal{F} < 0$ and a right-moving left-parabola LP(R) for $\mathcal{F} > 0$. These

passive drops are qualitatively close in shape to an upside down parabola but are asymmetric with a first moment of h that is non-zero (characteristic shapes shown in Fig. 1 (b)). The passive solutions are antisymmetric along the push/pull \mathcal{F} axis, and they move with opposite velocities that increase as the drop is squeezed (see Fig. 2(a)). All drops become longer and thinner as we move along the stretch/squeeze axis from squeeze to stretch, eventually reaching the region of drop breakup (DB), where the drop free surface reaches $h < 0$. For passive drops, we are able to show analytically (see SI at [43]) that for $\mathcal{F} = 0$, in this region no steady solutions exist that satisfy volume conservation. This argument can be extended to linear order in activity.

With activity, as shown in shown in Fig. 1 (c), we find, in addition to RP(L), LP(R) and DB, a right-moving right-parabola RP(R) state with finite traction, and then two long and thin states (see 2nd moment in Figs. 2 (c)), the right-moving double hump DH(R) state, which has a small dip followed by a prominent frontal hump, and the right-moving pancake PC(R) drop, which is flat almost everywhere with the average height $\bar{h} < h_0$. Both DH(R) and PC(R) drops have zero traction in the bulk (Fig. 2 (d)). The tractionless drops that we studied in [32] can be found in the DH(R) region of the phase plane along the line of equal contact angle (dotted line, Figs. 2 (b) - (d)). The symmetry about the push/pull axis is broken because the drop is motile at zero force due to the imposed winding $\omega = 1$ (Figs. 2 (b)). Both the RP(L) and LP(R) regions become smaller with activity and are pushed towards the top-left (push-left/squeeze) and top-right (push-right/squeeze) of the phase plane respectively by the emergence of the RP(R) phase, which largely occupies the middle squeeze region that lies between RP(L) and LP(R).

The stretch region of the phase plane is populated by DH(R) and PC(R), as well as DB. The region containing DH(R) and PC(R) shares a phase boundary with RP(R) determined by the second moment of h as a measure of the spread of the drop, and the distribution of substrate traction. The phase boundary is indicated in the schematic Fig. 1, as determined from the data in Figs. 2 (c) and (d). Strikingly, the transition between RP(R) and DH(R)/PC(R) is sharp suggesting a first order transition. The behaviour of the second moment and the drop velocity across the phase boundary is shown in Fig. 2 (e). There is a jump in both quantities going from RP(R) to DH(R) and also from DH(R) to RP(R). The change in drop shape induced by moving from RP(R) to DH(R) and back to RP(R) at constant squeeze $\mathcal{S} = 2$ is shown in Fig. 2 (f). The drop shape changes continuously within the DH(R) region but changes sharply at the phase boundary. There are also indications of bi-stability in the region: we have obtained two stable solutions for two different initial conditions at the same point in the phase plane (see SI at [43]). In contrast, the transition between DH(R) and PC(R) is smooth and happens under increased stretching for constant push (Fig. 2 (g)).

The drastic changes in drop shape that we have observed are not associated with changes in direction of motion. The active drop remains a right-parabola when its velocity is reversed at the RP(L)/RP(R) boundary. Stationary drop profiles are shown in Fig. 2 (h). Both passive and active drops are fastest for strong push and strong squeeze, towards the top corners of the phase plane. The drop slows down dramatically on entering the DH(R) region and continues to slow down as it enters the PC(R) region and approaches DB, however it does not stop before reaching DB.

For values of \mathcal{A} and f_{\pm} close to zero, the numerical solution is in good agreement with the analytic solution at linear order in \mathcal{A} and f_{\pm} . For constant squeeze and constant push, the relative error between the numerical solution and analytic solution decreases with activity (Fig. 3). The asymptotic solution remains a good approximation ($\sim 10\%$ relative error) when \mathcal{A} is of $\mathcal{O}(1)$ but only if drop is in one of the parabolic phases. The analytic solution ceases to be a good approximation for the more complex DH(R) and PC(R) drops.

In conclusion, we have studied the dynamics of a cell (an active LC drop) on a flat surface under external forces applied at its two ends. We have produced a phase dia-

gram in terms of the sum and differences of these forces and have shown how cell shape and motile behaviour is nonlinearly modulated by external forces. Our analysis has focused on one mechanism of motility driven by contractile/extensile active stresses. We expect that including other mechanisms [31] will change the locations of boundaries between the different phases we have observed. Clearly the changes in shape that we have observed here can be exploited to control behaviour of different cell phenotypes and tissue remodelling. The relation that we have derived between cell-substrate traction and forces, and between cell velocity and traction could be investigated by measuring the cell-substrate force using e.g. traction force microscopy and pushing/pulling the cell with a micropipette.

ACKNOWLEDGMENTS

Part of this work was funded by a Leverhulme Trust Research Project Grant RPG-2016-147. TBL acknowledges support of BrisSynBio, a BBSRC/EPSRC Advanced Synthetic Biology Research Centre (grant number BB/L01386X/1). SH acknowledges support of BBSRC grant BB/N009150/2.

-
- [1] B. Alberts, *Molecular Biology of the Cell* (W.W. Norton, 2017).
- [2] E. K. Paluch, I. M. Aspalter, and M. Sixt, Annual review of cell and developmental biology **32**, 469 (2016).
- [3] T. Lämmermann and M. Sixt, Current opinion in cell biology **21**, 636 (2009).
- [4] K. Chiou and E.-M. S. Collins, Developmental biology **433**, 155 (2018).
- [5] T. Lecuit and P.-F. Lenne, Nature reviews Molecular cell biology **8**, 633 (2007).
- [6] C. L. Chaffer and R. A. Weinberg, Science **331**, 1559 (2011).
- [7] T. Mitchison and L. Cramer, Cell **84**, 371 (1996).
- [8] D. A. Fletcher and R. D. Mullins, Nature **463**, 485 (2010).
- [9] F. Juelicher, K. Kruse, J. Prost, and J.-F. Joanny, Physics reports **449**, 3 (2007).
- [10] M. C. Marchetti, J.-F. Joanny, S. Ramaswamy, T. B. Liverpool, J. Prost, M. Rao, and R. A. Simha, Reviews of Modern Physics **85**, 1143 (2013).
- [11] E. L. Barnhart, K.-C. Lee, K. Keren, A. Mogilner, and J. A. Theriot, PLoS Biol **9**, e1001059 (2011).
- [12] A. B. Verkhovskiy, T. M. Svitkina, and G. G. Borisy, Current Biology **9**, 11 (1999).
- [13] P. T. Yam, C. A. Wilson, L. Ji, B. Hebert, E. L. Barnhart, N. A. Dye, P. W. Wiseman, G. Danuser, and J. A. Theriot, The Journal of cell biology **178**, 1207 (2007).
- [14] K. Keren, Z. Pincus, G. M. Allen, E. L. Barnhart, G. Marriott, A. Mogilner, and J. A. Theriot, Nature **453**, 475 (2008).
- [15] E. Anon, X. Serra-Picamal, P. Hersen, N. C. Gauthier, M. P. Sheetz, X. Trepat, and B. Ladoux, Proceedings of the National Academy of Sciences **109**, 10891 (2012).
- [16] E. Tjhung, A. Tiribocchi, D. Marenduzzo, and M. Cates, Nature communications **6**, 1 (2015).
- [17] C. Blanch-Mercader and J. Casademunt, Physical review letters **110**, 078102 (2013).
- [18] A. Callan-Jones, J.-F. Joanny, and J. Prost, Physical review letters **100**, 258106 (2008).
- [19] B. A. Camley, Y. Zhao, B. Li, H. Levine, and W.-J. Rappel, Physical Review E **95**, 012401 (2017).
- [20] K. Doubrovinski and K. Kruse, Physical review letters **107**, 258103 (2011).
- [21] I. Lavi, N. Meunier, R. Voituriez, and J. Casademunt, Physical Review E **101**, 022404 (2020).
- [22] R. J. Hawkins, M. Piel, G. Faure-Andre, A. Lennon-Dumenil, J. Joanny, J. Prost, and R. Voituriez, Physical review letters **102**, 058103 (2009).
- [23] E. Tjhung, D. Marenduzzo, and M. E. Cates, Proceedings of the National Academy of Sciences **109**, 12381 (2012).
- [24] D. Khoromskaia and G. P. Alexander, Physical Review E **92**, 062311 (2015).
- [25] L. Giomi and A. DeSimone, Physical review letters **112**, 147802 (2014).
- [26] R. J. Hawkins, R. Poincloux, O. Bénichou, M. Piel, P. Chavrier, and R. Voituriez, Biophysical journal **101**, 1041 (2011).
- [27] T. Sanchez, D. T. Chen, S. J. DeCamp, M. Heymann, and Z. Dogic, Nature **491**, 431 (2012).
- [28] M. Murrell, P. W. Oakes, M. Lenz, and M. L. Gardel, Nature reviews Molecular cell biology **16**, 486 (2015).
- [29] P. Pandya, J. L. Orgaz, and V. Sanz-Moreno, Current opinion in cell biology **48**, 87 (2017).

- [30] C. W. Wolgemuth, J. Stajic, and A. Mogilner, *Biophysical journal* **101**, 545 (2011).
- [31] A. Loisy, J. Eggers, and T. B. Liverpool, *Soft Matter* **16**, 3106 (2020).
- [32] A. Loisy, J. Eggers, and T. B. Liverpool, *Physical Review Letters* **123**, 248006 (2019).
- [33] Y.-J. Liu, M. Le Berre, F. Lautenschlaeger, P. Maiuri, A. Callan-Jones, M. Heuzé, T. Takaki, R. Voituriez, and M. Piel, *Cell* **160**, 659 (2015).
- [34] U. S. Schwarz and S. A. Safran, *Reviews of Modern Physics* **85**, 1327 (2013).
- [35] Y. Li, M. Wu, Z. Zhang, J. Xia, Z. Wang, X. Chen, X. Xiao, F. Lu, and Z. Dong, *Tissue Engineering Part A* **25**, 1614 (2019).
- [36] A. Saez, M. Ghibaudo, A. Buguin, P. Silberzan, and B. Ladoux, *Proceedings of the National Academy of Sciences* **104**, 8281 (2007).
- [37] B. L. Ricca, G. Venugopalan, S. Furuta, K. Tanner, W. A. Orellana, C. D. Reber, D. G. Brownfield, M. J. Bissell, and D. A. Fletcher, *Elife* **7**, e26161 (2018).
- [38] M. C. Marchetti, J.-F. Joanny, S. Ramaswamy, T. B. Liverpool, J. Prost, M. Rao, and R. A. Simha, *Reviews of Modern Physics* **85**, 1143 (2013).
- [39] F. Jülicher, S. W. Grill, and G. Salbreux, *Reports on Progress in Physics* **81**, 076601 (2018).
- [40] Y. Hatwalne, S. Ramaswamy, M. Rao, and R. A. Simha, *Physical review letters* **92**, 118101 (2004).
- [41] T. B. Liverpool and M. C. Marchetti, *Physical review letters* **97**, 268101 (2006).
- [42] A. Oron, S. H. Davis, and S. G. Bankoff, *Reviews of modern physics* **69**, 931 (1997).
- [43] See Supplementary information at [to be inserted].

The nonlinear motion of cells subject to external forces: Supplemental Material

I. ADDITIONAL PHASE DIAGRAMS

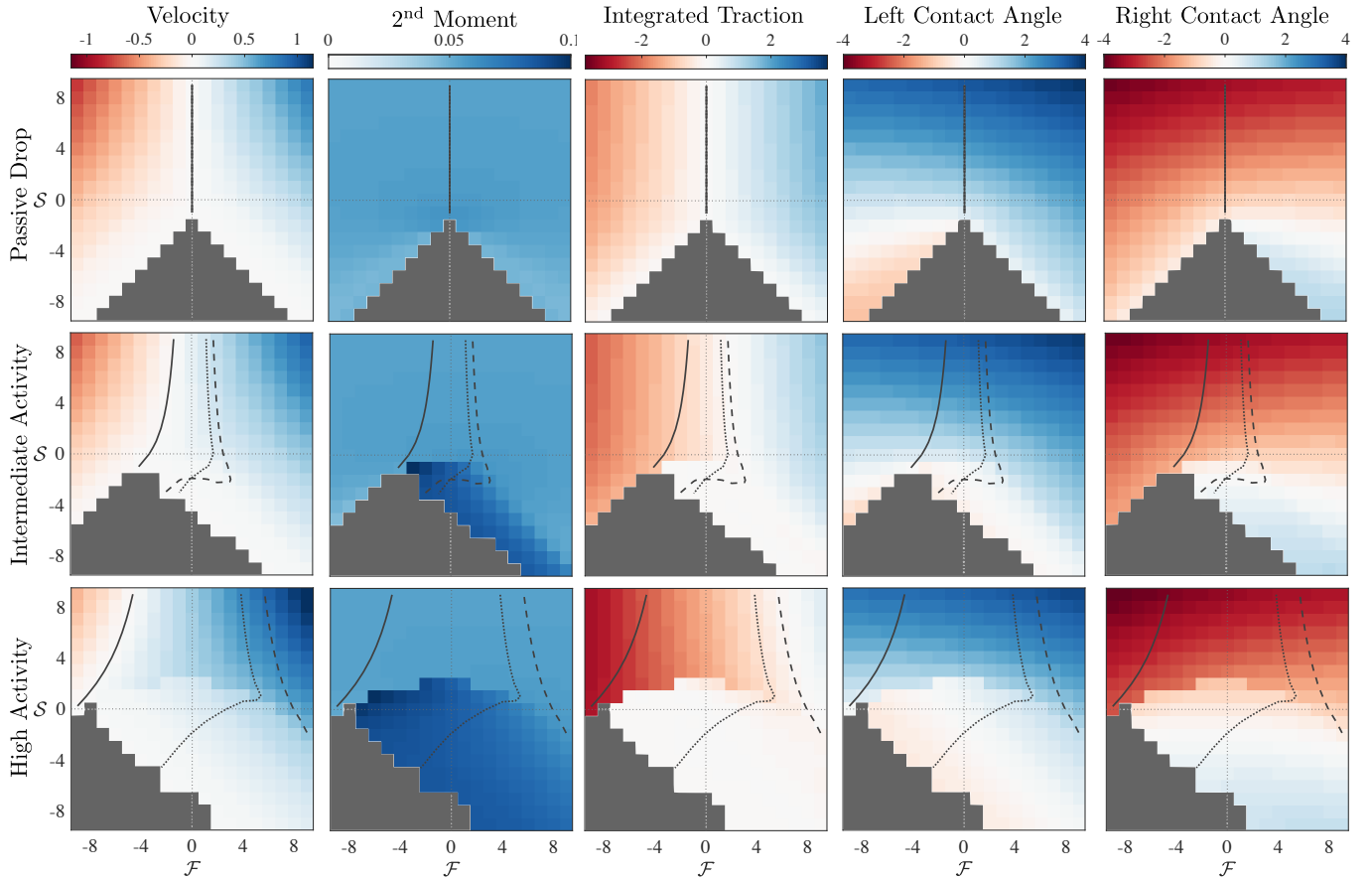


FIG. S1. First row: passive drop ($\mathcal{A} = 0$), second row: intermediate activity ($\mathcal{A} = 0.3$), third row: high activity ($\mathcal{A} = 1$). First column: drop velocity. Second column: 2nd moment $\int_{-L/2}^{L/2} (x - \mu_1)^2 h(x) dx$, where $\mu_1 = \int_{-L/2}^{L/2} x h(x) dx$. Third column: traction between the drop and the substrate integrated over 70% of the drop length. Fourth column: left contact angle $\phi_- = h'(-L/2)$, fifth column: right contact angle $\phi_+ = h'(L/2)$. The solid line in each plot is an isoline corresponding to zero velocity, the dotted line is an isoline corresponding to the drop having equal contact angles, and the dashed line is an isoline corresponding to the 1st moment $\mu_1 = 0$. The high activity phase diagrams have a $\mu_1 = 0$ isoline in the DH(R)/PC(R) region but this is not included here.

II. DERIVING THE HEIGHT EQUATION

We begin with the force balance equation in the lubrication approximation

$$\partial_{\tilde{x}} \tilde{p} - \tilde{f}_{\tilde{x}} = \eta \partial_{\tilde{z}}^2 \tilde{u} - \tilde{\alpha} \partial_{\tilde{z}} (n_x n_z) = \partial_{\tilde{z}} \tilde{\sigma}_{\tilde{x}\tilde{z}}, \quad (\text{S1a})$$

$$\partial_{\tilde{z}} \tilde{p} = 0, \quad (\text{S1b})$$

where we have chosen

$$\tilde{f}_{\tilde{x}} = \tilde{f}_+ \delta(\tilde{x} - \frac{\tilde{L}}{2}) + \tilde{f}_- \delta(\tilde{x} + \frac{\tilde{L}}{2}), \quad \tilde{f}_{\tilde{z}} = 0. \quad (\text{S2})$$

For here, we will **omit the tildes**, but note that the quantities in this section are **not** non-dimensionalised. The strategy will be to first integrate (S1a) at $\pm L/2$ to get boundary conditions on $p(\pm L/2)$ imposed by the Dirac deltas. We will then solve (S1a) away from $x = \pm L/2$, and apply the derived boundary conditions at $\pm L/2$.

A. Integrating at the boundaries

At $x = L/2$, we have

$$\int_{\frac{L}{2}-\Delta}^{\frac{L}{2}+\Delta} \partial_x p dx - f_+ \int_{\frac{L}{2}-\Delta}^{\frac{L}{2}+\Delta} \delta(x - \frac{L}{2}) dx - f_- \int_{\frac{L}{2}-\Delta}^{\frac{L}{2}+\Delta} \delta(x + \frac{L}{2}) dx = \int_{\frac{L}{2}-\Delta}^{\frac{L}{2}+\Delta} \partial_z \sigma_{xz} dx.$$

The last term on the LHS vanishes because of the definition of the delta function and the term on the RHS vanishes as we shrink the integration region ($\Delta \rightarrow 0^+$) because the integrand is continuous. The procedure is identical at $x = -L/2$. Thus we have

$$p(\frac{L}{2} + \Delta) - p(\frac{L}{2} - \Delta) - f_+ = 0, \quad p(-\frac{L}{2} + \Delta) - p(-\frac{L}{2} - \Delta) - f_- = 0.$$

We model the system to have a uniform pressure $\pi_0 + \pi_{ref}$, where π_{ref} is an arbitrary reference pressure while π_0 is the uniform pressure that is present in the absence of activity α and external forces F_{\pm} , where the drop is stationary and symmetric. Because the external force is localised to $x = \pm L/2$ and we take the pressure to be uniform everywhere else outside the drop, it must be the case that $p(\frac{L}{2} + \Delta) = p(-\frac{L}{2} - \Delta) = \pi_0 + \pi_{ref}$. We also define

$$p(L/2) = \lim_{\Delta \rightarrow 0^+} p(L/2 - \Delta), \quad p(-L/2) = \lim_{\Delta \rightarrow 0^+} p(-L/2 + \Delta),$$

resulting in the boundary conditions

$$p(\frac{L}{2}) = \pi_0 + \pi_{ref} - f_+, \quad (\text{S3a})$$

$$p(-\frac{L}{2}) = \pi_0 + \pi_{ref} + f_-. \quad (\text{S3b})$$

Solving equation (S1a) is now equivalent to solving

$$\partial_x p = \partial_z \sigma_{xz} \quad (\text{S4})$$

with boundary conditions (S3).

B. Pressure as a functional of drop height

The pressure $p(x)$ inside the drop can be related to the drop height $h(x)$ using the normal component of the free surface boundary condition (see main text)

$$\mathbf{m} \cdot \boldsymbol{\sigma} \cdot \mathbf{m} = \gamma \kappa - \pi_{ref}.$$

Using the scalings from the lubrication approximation, $\alpha \sim \epsilon^{-1}$, $p \sim \epsilon^{-2}$, $u \sim 1$, and $w \sim \epsilon$ (from incompressibility), $\sigma_{xx} = \sigma_{zz} \approx -p \sim \epsilon^{-2}$, $\sigma_{xz} \sim \epsilon^{-1}$, we can write the LHS of the above equation as

$$\begin{aligned} \mathbf{m} \cdot \boldsymbol{\sigma} \cdot \mathbf{m} &= m_x \sigma_{xz} m_z + m_z \sigma_{xz} m_x + m_z \sigma_{zz} m_z + m_x \sigma_{xx} m_x \\ &\approx \frac{1}{1 + (h')^2} (-p(h')^2 - p - 2h' \sigma_{xz}) \\ &= -p - 2 \frac{h' \sigma_{xz}}{1 + (h')^2} \\ &\approx -p. \end{aligned}$$

Approximating κ to leading order, we have

$$\begin{aligned} \kappa &= \frac{h''}{(1 + (h')^2)^{\frac{3}{2}}} \\ &\approx h''. \end{aligned}$$

Thus

$$p(x) = -\gamma h'' + \pi_{ref}. \quad (\text{S5})$$

C. Height equation

To get an ODE for $h(x)$ we apply a travelling wave condition to the kinematic boundary condition at the free surface of the drop. Because of the nature of the problem, we first need to integrate equation (S4) in order to apply the boundary conditions on the pressure (S3). After doing this, we use the relation between the pressure and the second derivative of $h(x)$ (S5) to obtain an integro-differential equation for $h(x)$. Finally, we differentiate said integro-differential equation to obtain an ordinary differential equation for $h(x)$.

The kinematic boundary condition is written

$$\partial_t h + u \partial_x h - w = 0,$$

and it comes from requiring $\frac{D}{Dt}(h(x, t) - z) = 0$, where $\frac{D}{Dt} = \partial_t + \mathbf{u} \cdot \nabla$. We impose a travelling wave solution $h = h(x - Vt)$, where V is the unknown constant drop velocity. Substituting the travelling wave condition into the kinematic boundary condition gives the expression

$$\int_0^{h(x)} u dz = Vh, \quad (\text{S6})$$

where we have made the transformation $x \leftarrow x - Vt$, so that now x is the centre of mass coordinate. To obtain the fluid velocity field u , we integrate (S4) twice with respect to z and use the partial slip boundary condition at the substrate and the tangential component of the free surface boundary condition (see main text) (which can be re-written as a condition on $\partial_z u(z = h)$). The fluid velocity field u is then given by

$$u = \frac{\alpha h}{4\pi\omega\eta} \left(1 - \cos \frac{2\omega\pi z}{h} \right) + \frac{\partial_x p}{\eta} \left(\frac{z^2}{2} - h(z + l_u) \right). \quad (\text{S7})$$

Substituting (S7) into (S6) and isolating the pressure gradient yields

$$\partial_x p = \frac{\eta(\tilde{\alpha}h - V)}{\frac{1}{3}h^2 + l_u h}, \quad (\text{S8})$$

where $\tilde{\alpha} = \frac{\alpha}{4\pi\omega\eta}$. From here the strategy will be to integrate (S8) and apply the boundary conditions (S3) in order to determine the integration constant and the unknown drop velocity V . We find that the drop velocity is given by

$$\eta V = \frac{\int_{-\frac{L}{2}}^{\frac{L}{2}} \frac{\eta\tilde{\alpha}}{\frac{1}{3}h + l_u} dx + (f_+ + f_-)}{\int_{-\frac{L}{2}}^{\frac{L}{2}} \frac{1}{\frac{1}{3}h^2 + l_u h} dx}. \quad (\text{S9})$$

As a sanity check, we see that the second term in the numerator vanishes when the forces are equal and opposite, which means that the drop velocity is unchanged by the forces when they cancel each other out. This is good. The drop velocity also vanishes when the activity α and both forces vanish, which is good. After some algebra, and taking advantage of the fact that we can obtain two equivalent expressions for pressure by integrating (S8) from $-\frac{L}{2}$ to x or from x to $\frac{L}{2}$, we arrive find that the pressure is given by

$$p(x) = \pi_0 + \pi_{ref} - \frac{f_+ - f_-}{2} + \frac{1}{2} \int_{-L/2}^x \frac{\eta\tilde{\alpha}}{\frac{1}{3}h + l_u} dy + \frac{1}{2} \int_{L/2}^x \frac{\eta\tilde{\alpha}}{\frac{1}{3}h + l_u} dy - \frac{1}{2} \left(\frac{f_+ + f_- + \eta\tilde{\alpha}I_1}{I_2} \right) \left(\int_{-L/2}^x \frac{1}{\frac{1}{3}h^2 + l_u h} dy + \int_{L/2}^x \frac{1}{\frac{1}{3}h^2 + l_u h} dy \right), \quad (\text{S10})$$

where

$$I_1 = \int_{-L/2}^{L/2} \frac{1}{\frac{1}{3}h + l_u} dy, \quad I_2 = \int_{-L/2}^{L/2} \frac{1}{\frac{1}{3}h^2 + l_u h} dy.$$

Using the relation between the pressure and the second derivative of the drop height (S5), we can write (S10) as an integro-differential equation that is independent of the reference pressure

$$-\gamma h'' = \pi_0 - \frac{f_+ - f_-}{2} + \frac{1}{2} \int_{-L/2}^x \frac{\eta\tilde{\alpha}}{\frac{1}{3}h + l_u} dy + \frac{1}{2} \int_{L/2}^x \frac{\eta\tilde{\alpha}}{\frac{1}{3}h + l_u} dy - \frac{1}{2} \left(\frac{f_+ + f_- + \eta\tilde{\alpha}I_1}{I_2} \right) \left(\int_{-L/2}^x \frac{1}{\frac{1}{3}h^2 + l_u h} dy + \int_{L/2}^x \frac{1}{\frac{1}{3}h^2 + l_u h} dy \right). \quad (\text{S11})$$

Finally, we can obtain an ordinary differential equation by differentiating (S11) to obtain

$$\frac{\gamma h'''}{\eta} \left(\frac{1}{3} h^3 + l_u h^2 \right) + \frac{\alpha h^2}{4\pi\omega\eta} = \frac{1}{\eta} \left(\frac{I_1 + (f_+ + f_-)}{I_2} \right) h, \quad (\text{S12})$$

where the drop velocity V is the pre-factor of h on the RHS.

III. SOLVING THE HEIGHT EQUATION WITH THE CRANK-NICHOLSON METHOD

The equation that is fed into the Crank-Nicholson algorithm is

$$\partial_t h + \partial_x (-\mathcal{V}h + h'''(\frac{1}{3}h^3 + l_u h^2) + \mathcal{A}h^2) = 0, \quad (\text{S13})$$

where the drop velocity \mathcal{V} is defined in the main text. Equation (S13) is subject to the constraints

$$\int_{-L/2}^{L/2} h(x) dx = \Omega, \quad h(\pm L/2) = h_0, \quad (\text{S14})$$

where Ω is the dimensionless drop volume, and

$$h''(-L/2) + \pi_0 + f_- = 0, \quad h''(L/2) + \pi_0 - f_+ = 0, \quad (\text{S15})$$

with

$$\pi_0 = \frac{2\phi}{-\frac{3h_0}{\phi} + \sqrt{\frac{9h_0^2}{\phi^2} + \frac{6\Omega}{\phi}}},$$

where ϕ is the re-scaled contact angle.

Equation (S13) is of the form $\partial_t h = I$, where I represents the second term on the LHS of (S13). The Crank-Nicholson scheme advances in time according to

$$\frac{h_i^{n+1}}{\Delta t} - \frac{1}{2} I_i(\mathbf{X}^{n+1}) = \frac{h_i^n}{\Delta t} + \frac{1}{2} I_i(\mathbf{X}^n), \quad (\text{S16})$$

where the subscripts refer to the spatial discretisation and the superscripts refer to the time discretisation. Note that in the second term on the LHS, $I_i(\mathbf{X}^{n+1})$, means I evaluated at spatial point i at time-step $n + 1$.

A. Spatial discretisation

For the discretisation we use the substitution $x = Ly$, with L being the drop length, and discretise the domain $y \in [-0.5, 0.5]$ with uniform grid spacing Δy . The stiff term is discretised as follows

$$\partial_x \left(h'' \left(\frac{1}{3} h^3 + l_u h^2 \right) \right) \rightarrow \frac{\left[\left(\frac{1}{3} h_i^3 + l_u h_i^2 \right) + \left(\frac{1}{3} h_{i+1}^3 + l_u h_{i+1}^2 \right) \right] (h_{i+2} - 3h_{i+1} + 3h_i - h_{i-1})}{2L^4 \Delta y^4} - \frac{\left[\left(\frac{1}{3} h_{i-1}^3 + l_u h_{i-1}^2 \right) + \left(\frac{1}{3} h_i^3 + l_u h_i^2 \right) \right] (h_{i+1} - 3h_i + 3h_{i-1} - h_{i-2})}{2L^4 \Delta y^4},$$

and all other terms are discretised as

$$\partial_x g(h) \rightarrow \frac{g(h_{i+1}) - g(h_{i-1})}{2L\Delta y},$$

where $g(h) = Ah^2$ for the active term, and $g(h) = \frac{AI_1 + (f_+ + f_-)}{I_2} h$ for the velocity term.

B. Algorithm and boundary conditions

Equation (S16) leads to a set of nonlinear algebraic equations for $\{h_i^{n+1}\}$, where $\{h_i^n\}$ are known, which is solved using the Matlab fsolve algorithm. For N spatial grid points, define $\mathbf{X}^{n+1} = (h_1, \dots, h_N)^{n+1}$. The algorithm solves $\mathbf{F}(\mathbf{X}^{n+1}) = \mathbf{0}$ with

$$\mathbf{F}(\mathbf{X}^{n+1}) = \frac{\mathbf{X}^{n+1}}{\Delta t} - \frac{1}{2}\mathbf{I}(\mathbf{X}^{n+1}) - \frac{\mathbf{X}^n}{\Delta t} - \frac{1}{2}\mathbf{I}(\mathbf{X}^n) \quad i = 3, \dots, N-2, \quad (\text{S17})$$

where $\mathbf{I} = (I_1, \dots, I_N)$, with I_i being the spatial differential operator evaluated at spatial point i . The boundary conditions are implemented using grid points 1, 2, $N-1$, N . The condition on the drop height at $\pm L/2$ is implemented as

$$F_1 = h_1^{n+1} - h_0 \quad (\text{S18a})$$

$$F_N = h_N^{n+1} - h_0. \quad (\text{S18b})$$

The boundary conditions on the second derivative (S15) are implemented using finite difference coefficients to approximate the second derivative:

$$F_2 = \frac{2h_1^{n+1} - 5h_2^{n+1} + 4h_3^{n+1} - h_4^{n+1}}{\Delta y^2} + L^2 \left(\frac{\pi_0 + f_-}{\tilde{C}} \right), \quad (\text{S19a})$$

$$F_{N-1} = \frac{2h_N^{n+1} - 5h_{N-1}^{n+1} + 4h_{N-2}^{n+1} - h_{N-3}^{n+1}}{\Delta y^2} + L^2 \left(\frac{\pi_0 - f_+}{\tilde{C}} \right). \quad (\text{S19b})$$

Once equation (S13) is discretised, we use a nonlinear solver (MATLAB's "fsolve") for the simultaneous equations $\mathbf{F}(\mathbf{X}^{n+1}) = \mathbf{0}$, with the components of \mathbf{F} given by (S17), (S18), and (S19). We also calculate the Jacobian $\partial F_i / \partial h_j$ explicitly and supply it to the nonlinear solver. The algorithm begins with a user set initial condition \mathbf{X}^1 which is chosen to satisfy the boundary conditions on drop height but not necessarily the boundary conditions on the second derivative. The drop velocity \mathcal{V} as well as the drop length L are calculated iteratively starting from the initial condition (the drop length is derived from the constraint that the drop has a constant volume) and plugged into the Crank-Nicholson evolution equation which is solved for \mathbf{X}^2 . This process is repeated until steady state is reached i.e. the difference between \mathbf{X}^{n+1} and \mathbf{X}^n is less than some tolerance.

IV. ASYMPTOICS

We expand the equation

$$h'''(\frac{1}{3}h^3 + l_u h^2) + \mathcal{A}h^2 = \left(\frac{\mathcal{A}I_1 + (f_+ + f_-)}{I_2} \right) h, \quad (\text{S20})$$

where $I_1 = \int_{-L/2}^{L/2} (\frac{1}{3}h + l_u)^{-1} dx$ and $I_2 = \int_{-L/2}^{L/2} (\frac{1}{3}h^2 + l_u h)^{-1} dx$, for small activity and small forces.

A. Small forces and small activity

We consider small perturbations to a symmetric passive drop by expanding $h(x)$ to linear order in f_{\pm} and \mathcal{A} around the passive solution, obtained by setting $f_+ = f_- = 0$ and $\mathcal{A} = 0$ in (S20) and either imposing $h''(x) = \pi_0$ or $h'(\frac{\pm L}{2}) = \mp \phi$ along with $h(\frac{\pm L}{2}) = h_0$:

$$h_p = -\frac{\phi L}{4} \left(\frac{4x^2}{L^2} - 1 \right) + h_0. \quad (\text{S21})$$

We also expand L to linear order in f_{\pm} and \mathcal{A} :

$$L = L_p - f_+ L_+ - f_- L_- + \mathcal{A} L_{\alpha} + \dots \quad (\text{S22})$$

which leads to

$$h(y) = H_0 + f_+ \left(\frac{\phi L_+}{4} (y^2 - 1) - h_+ \right) + f_- \left(\frac{\phi L_-}{4} (y^2 - 1) - h_- \right) + \mathcal{A} \left(h_\alpha - \frac{\phi L_\alpha}{4} (y^2 - 1) \right) + \dots \quad (\text{S23})$$

where $y = 2x/L$, $H_0 = -\frac{\phi L_p}{4} (y^2 - 1) + h_0$, and L_p is the length of the passive drop given by $L_p = \sqrt{\frac{6\Omega}{\phi} + \frac{9h_0^2}{\phi^2}} - \frac{3h_0}{\phi}$ for a drop of volume Ω . Substituting (S23) into (S20) and keeping terms only to linear order yields three differential equations at $\mathcal{O}(f_+)$, $\mathcal{O}(f_-)$, and $\mathcal{O}(\mathcal{A})$ that can be integrated for h_\pm and h_α . At $\mathcal{O}(f_+)$ we have

$$h_+'''(x) \left(\frac{1}{3} H_0^2 + l_u H_0 \right) = -\frac{1}{I_2}, \quad h_+(\pm 1) = 0, \quad h_+''(1) = -\frac{L_p^2}{4} - \frac{\phi L_+}{2}. \quad (\text{S24})$$

For consistency, we must have also $h_+''(-1) = -\phi L_+/2$ but we cannot impose this on the equation, as there are already three boundary conditions. Fortunately, it falls out automatically because the integrals I_1 and I_2 encode both boundary conditions on h'' . At $\mathcal{O}(f_-)$ we have

$$h_-'''(x) \left(\frac{1}{3} H_0^2 + l_u H_0 \right) = -\frac{1}{I_2}, \quad h_-(\pm 1) = 0, \quad h_-''(-1) = \frac{L_p^2}{4} - \frac{\phi L_-}{2}. \quad (\text{S25})$$

Again, for consistency, we must have $h_-''(1) = -\phi L_-/2$, which again falls out automatically. At $\mathcal{O}(\mathcal{A})$ we have

$$h_\alpha'''(x) \left(\frac{1}{3} H_0^2 + l_u H_0 \right) = \frac{I_1}{I_2} - H_0, \quad h_\alpha(\pm 1) = 0, \quad h_\alpha''(1) = -\frac{\phi L_\alpha}{2}. \quad (\text{S26})$$

For consistency we must have $h_\alpha''(-1) = -\phi L_\alpha/2$, which falls out automatically. To perform the integration, we use the variable $y = \frac{2x}{L}$. It is useful to define the following function

$$G_f(y) = \left(1 + \frac{y}{\sqrt{1+4h_0/\phi L_p}} \right)^2 \log \left(1 + \frac{y}{\sqrt{1+4h_0/\phi L_p}} \right) - \left(1 - \frac{y}{\sqrt{1+4h_0/\phi L_p}} \right)^2 \log \left(1 - \frac{y}{\sqrt{1+4h_0/\phi L_p}} \right) + \frac{1}{\beta \phi} \left[\left(\beta - \frac{\phi y}{\sqrt{1+4h_0/\phi L_p}} \right)^2 \log \left(\beta - \frac{\phi y}{\sqrt{1+4h_0/\phi L_p}} \right) - \left(\beta + \frac{\phi y}{\sqrt{1+4h_0/\phi L_p}} \right)^2 \log \left(\beta + \frac{\phi y}{\sqrt{1+4h_0/\phi L_p}} \right) \right],$$

where

$$\beta = \sqrt{\frac{1 + \frac{4h_0}{\phi L_p} + \frac{12l_u}{\phi L_p}}{1 + \frac{4h_0}{\phi L_p}}}.$$

We also need

$$G_\alpha(y) = \frac{\phi}{4\beta} \left[\left(\frac{\beta}{\phi} + \frac{y}{\sqrt{1+4h_0/\phi L_p}} \right)^2 \log \left(\frac{\beta}{\phi} + \frac{y}{\sqrt{1+4h_0/\phi L_p}} \right) - \left(\frac{\beta}{\phi} - \frac{y}{\sqrt{1+4h_0/\phi L_p}} \right)^2 \log \left(\frac{\beta}{\phi} - \frac{y}{\sqrt{1+4h_0/\phi L_p}} \right) \right].$$

In terms of these functions, the leading order contributions to the drop height are

$$h_+(y) = \frac{-L_p^2(1 + \frac{4h_0}{\phi L_p})}{8G_f''(1)} \left[G_f(y) + \frac{1}{2} G_f''(1) \left(1 + \frac{4\phi}{L} L_p^2 \right) y^2 - \sqrt{1 + \frac{4h_0}{\phi L_p}} G_f(1) y - \frac{G_f''(1)(1 + 4\phi L_+/L_p^2)}{2(1 + 4h_0/\phi L_p)} \right], \quad (\text{S27a})$$

$$h_-(y) = \frac{-L_p^2(1 + \frac{4h_0}{\phi L_p})}{8G_f''(1)} \left[G_f(y) - \frac{1}{2} G_f''(1) \left(1 - \frac{4\phi L_-}{L_p^2} \right) y^2 - \sqrt{1 + \frac{4h_0}{\phi L_p}} G_f(1) y + \frac{G_f''(1)(1 - 4\phi L_-/L_p^2)}{2(1 + 4h_0/\phi L_p)} \right], \quad (\text{S27b})$$

$$h_\alpha(y) = \frac{3L_p^2 \sqrt{1 + \frac{4h_0}{\phi L_p}}}{2\phi} \left[\frac{G_\alpha''(1)}{G_f''(1)} G_f(y) - G_\alpha(y) + \sqrt{1 + \frac{4h_0}{\phi L_p}} \left(G_\alpha(1) - \frac{G_\alpha''(1)}{G_f''(1)} G_f(1) \right) y \right], \quad (\text{S27c})$$

where

$$L_+ = \frac{-L_p^3}{24} \left(\frac{\phi L_p}{2} + h_0 \right)^{-1}, \quad (\text{S28a})$$

$$L_- = \frac{L_p^3}{24} \left(\frac{\phi L_p}{2} + h_0 \right)^{-1}, \quad (\text{S28b})$$

$$L_\alpha = 0. \quad (\text{S28c})$$

V. CRITERION FOR DROP BREAK-UP AT ZERO NET FORCE

Consider a passive drop with $\mathcal{A} = 0$ and $\mathcal{F} = 0$. The equation for drop height becomes

$$h'''(\frac{1}{3}h^3 + l_u h^2) = 0 \quad (\text{S29})$$

and has the solution

$$h = -\frac{1}{2} \left(\pi_0 + \frac{\mathcal{S}}{2} \right) \left(x^2 - \frac{L^2}{4} \right) + h_0, \quad (\text{S30})$$

where we have used $h(\pm L/2) = h_0$ and $h'' = f_+ - \pi_0$. The drop length L is determined by the volume constraint $\int_{-L/2}^{L/2} h dx = \Omega > 0$. The drop length diverges at $\mathcal{S} = -2\pi_0 \approx -1.99$ (π_0 is chosen so that the contact angle of a passive drop is one), and goes negative for $\mathcal{S} < -2\pi_0$. This means that volume conservation is not truly satisfied even though the condition $\int_{-L/2}^{L/2} h dx = \Omega$ is satisfied mathematically by a negative L . This is clear in the left plot in figure S2, where $h < 0$ for $\mathcal{S} < -2\pi_0$ and thus $\int_{-|L|/2}^{|L|/2} h dx < 0$, with $|L|$ being the actual length of the drop. The critical value of $\mathcal{S} = -2\pi_0$ is consistent with what we see on the phase diagrams: the DB region for a passive drop begins between $\mathcal{S} = -1$ and $\mathcal{S} = -2$ along the line $\mathcal{F} = 0$ (see main text).

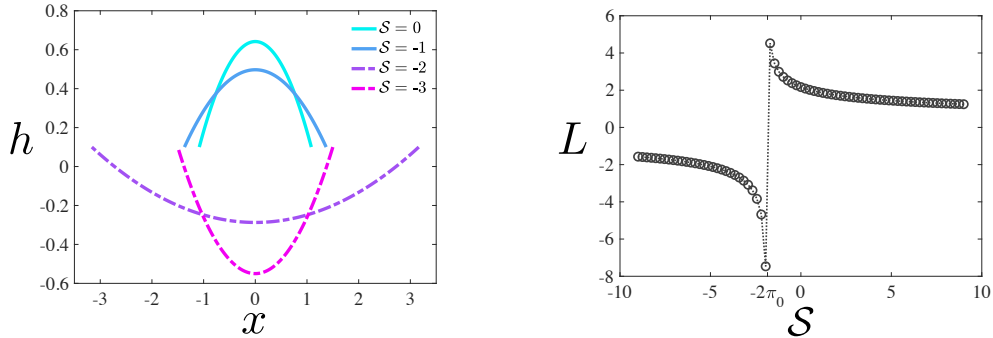


FIG. S2. Left: droplet height profiles at $\mathcal{F} = 0$ and $\mathcal{A} = 0$. Here, $\pi_0 = 0.9226$ and $\Omega = 1$. Right: drop length L as a function of \mathcal{S} .

VI. DIFFERENT STEADY STATES RESULTING FROM DIFFERENT INITIAL CONDITIONS

Our model is capable of producing different steady state drop profiles for the same activity and applied forces starting from different height profiles in the iterative Crank-Nicholson algorithm. This is shown in figure S3.

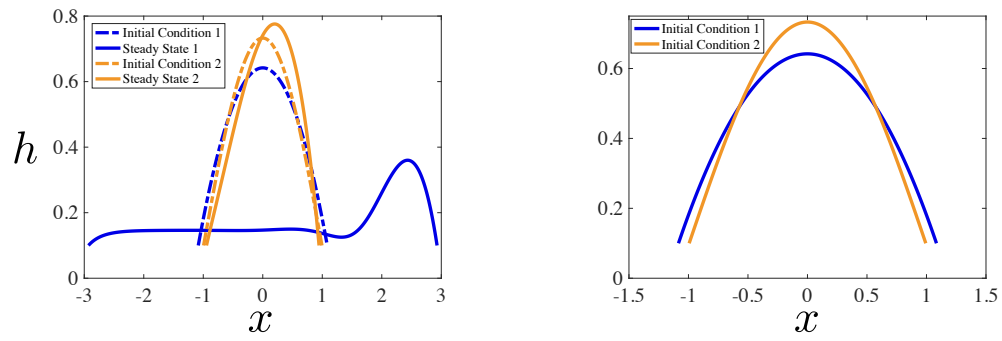


FIG. S3. Left: Initial height profiles (dashed lines) and steady state profiles (solid lines) for Right: Only the initial height profiles.